Spectral characterization of an industrial EUV light source for nanolithography

OPEN ACCESS
IOP Publishing
Journal of Physics D: Applied Physics
J. Phys. D: Appl. Phys. **53** (2020) 055204 (7pp)
https://doi.org/10.1088/1361-6463/ab56d4

Spectral characterization of an industrial EUV light source for nanolithography

F Torretti[1,2], F Liu[3], M Bayraktar[4], J Scheers[1,2], Z Bouza[1], W Ubachs[1,2], R Hoekstra[1,5] and O Versolato[1]

[1] Advanced Research Center for Nanolithography, Science Park 106, 1098 XG Amsterdam, The Netherlands
[2] Department of Physics and Astronomy, and LaserLaB, Vrije Universiteit, De Boelelaan 1081, 1081 HV Amsterdam, The Netherlands
[3] ASML Netherlands B.V., De Run 6501, 5504 DR Veldhoven, The Netherlands
[4] Industrial Focus Group XUV Optics, MESA+ Institute for Nanotechnology, University of Twente, Drienerlolaan 5, 7522 NB Enschede, The Netherlands
[5] Zernike Institute for Advanced Materials, University of Groningen, Nijenborgh 4, 9747 AG Groningen, The Netherlands

E-mail: fei.liu@asml.com, m.bayraktar@utwente.nl and o.versolato@arcnl.nl

Received 8 August 2019, revised 30 October 2019
Accepted for publication 12 November 2019
Published 28 November 2019

Abstract

The emission spectra from an industrial, droplet-based, laser-produced plasma, extreme ultraviolet light source for nanolithography are here presented and analyzed. The dependence of spectral features on the CO_2-drive-laser intensity is studied by changing the beam spot size at constant pulse energy and duration. We characterize the spectrum by fitting the results of atomic structure calculations to the short-wavelength region (7–11 nm), where the contributions from various charge states can be resolved, and obtain the relative contributions of charge states Sn^{9+}–Sn^{15+}. These relative contributions are compared to charge state populations as calculated with the non-equilibrium plasma kinetics code FLYCHK. The calculations are shown to be in good qualitative agreement with the results, showing that the effective plasma temperature, and with it, the shape of the unresolved, main emission feature at 13.5 nm, is a remarkably weak function of laser intensity under this source normal operating conditions.

Keywords: spectroscopy, laser-produced plasma, EUV source

(Some figures may appear in colour only in the online journal)

1. Introduction

Extreme ultraviolet (EUV) lithography [1, 2] is the main candidate for replacement of current 193 nm immersion lithography [3–7], with further miniaturization, fewer processing steps enabled by the shorter wavelength of the radiation. In nanolithographic applications, EUV radiation is generated using laser-produced plasma (LPP) light sources. Several other approaches for generating EUV light were considered [8, 9], but the requirement for mass-limited targets, their superior brightness has established droplet-based LPP as the de facto high-power industrial EUV sources [10, 11]. In state-of-the-art industrial LPP, molten tin micro-droplets are first pre-deformed into disk-like targets by a low-intensity laser *prepulse*, in order to ensure optimal coupling with the following high-intensity (10^9–10^{10} W cm^{-2}) *main pulse*. The resultant hot, high density LPP efficiently emits EUV radiation around 13.5 nm due to the atomic line emission from the highly-charged Sn^{9+}–Sn^{14+} ions [12–20]. This radiation conveniently overlaps with the peak reflectivity of molybdenum-silicon multi-layer mirrors [21, 22], characterized by a 2% reflectivity bandwidth centered at 13.5 nm wavelength,

employed as projection optics in EUV lithography scanners [1]. On the path towards high-volume EUV lithography, source characterization, physical understanding, improvement are important targets [23]. Amongst other techniques, spectroscopic measurements of the source emission spectrum are a powerful tool to diagnose source conditions [24]. Moreover, the projection optics [1], EUV pellicle [25] in the scanner are sensitively dependent on the spectral emission characteristics as, e.g. the out-of-band EUV spectrum, i.e. photons outside the 2% reflection bandwidth, may influence coating lifetime, further introduce undesirable thermal effects [26, 27].

We present spectra obtained from an industrial LPP EUV light source. The analysis revolves around the short wavelength emission features found in the 7–11 nm range. The result of atomic structure calculations given in [28] are used to characterize the charge state contribution to the spectrum by employing a fitting procedure. Using the non-equilibrium plasma kinetics code FLYCHK [29], the fit results are compared to the calculated charge state populations, thus obtaining an effective plasma temperature, scaling thereof with laser intensity.

2. Experiment

The plasma emission spectra have been acquired from an industrial ASML 'S2' EUV source driven by a 10.6 μm-wavelength CO_2-gas-laser [30] with EUV power of 100 W at the intermediate focus, i.e. the power delivered by the source to the scanner (see figure 1). The source is operated with a repetition rate of 50 kHz, with Sn droplets of 20–30 μm in diameter [6]. The initially-spherical droplet is pre-deformed into a thin, disk-like target about 300 μm in diameter using a 10 μm laser *prepulse* of few tens of mJ. This prepulse is followed by a 10 μm, high-energy, high-intensity *main pulse* which creates the plasma necessary for EUV emission. The main pulse energy is kept constant throughout the experiments at approximately 500 mJ. Its temporal profile also remains unchanged, which exhibits a strong peak decaying over a several-10 ns time scale. In order to probe different plasma temperatures,, therefore charge state populations, the main pulse beam-size on target is scanned by changing the position of the last optical elements along the laser propagation direction. This operation results in the main pulse beam-spot at Sn target being monotonically scanned, going from approximately 200 μm–400 μm diameter. Changes in the spatial size of the main pulse will affect its intensity, the parameter pertinent for setting plasma temperature [31]. In the rest of this article, due to the fact that the laser-pulse duration remains unchanged, average laser fluence at the target will be employed as the relevant quantity. In the performed scan, the fluence is varied between approximately 300 J cm^{-2}–800 J cm^{-2}. The total EUV energy in the 2% band at the intermediate focus per pulse is in the range of 2.5 mJ–2.8 mJ.

Throughout the experiment, while the laser beam-spot is changed, the source is operated to maximize in-band EUV output for each given experimental condition. This is achieved by adjusting the alignment of the droplet, prepulse laser in the plane perpendicular to laser propagation direction. By adjusting alignment between the droplet, the prepulse, the disk-like target will exhibit a tilt with respect to the main pulse propagation direction [32]. Due to this tilt, the cylindrical symmetry of the main pulse-target interaction is broken,, the spectral emission may be expected to suffer from anisotropy. Angular dependence of the EUV emission in the 2% band in this type of sources is a well-established fact, even in perfectly cylindrically-symmetric interactions [24, 33]; moreover, there are no studies dedicated to the investigation of the anisotropy of the full EUV emission spectrum. Therefore, dedicated measurements were performed to study the aforementioned angular properties and, more precisely, the effects of the optimization procedure. Keeping all other parameters constant, the laser-to-droplet alignment is changed as performed during the optimization procedure. The resulting target tilt is inspected using a shadowgraphic technique [34], imaging the Sn disk at 90° with respect to the laser direction. Anisotropy of the emission after irradiating the tilted targets with the main pulse was found to mainly affect the total amount of radiation emitted but has negligible impact on the spectral characteristics of the emission. Figure 2 shows the relative emission spectra obtained for three distinct target tilts, illustrated by the shadowgraphic images in the figure legend.

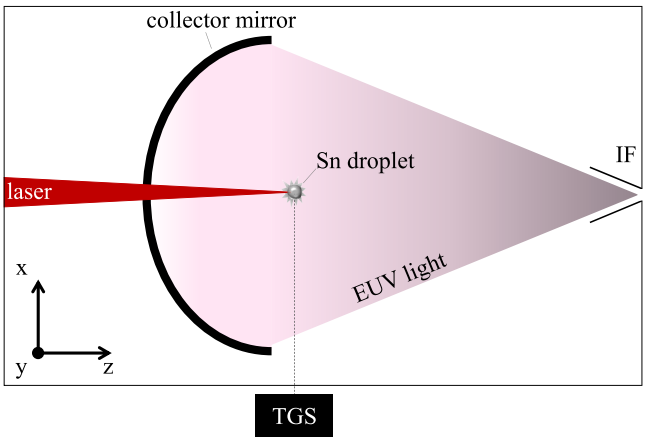

Figure 1. Simplified schematic representation of the EUV source around the time of prepulse laser impact. Sn droplets are travelling in the negative-y direction. The transmission-grating spectrometer (TGS) is positioned at a 90° angle with respect to the drive laser light propagation direction. The intermediate focus (IF) is the interface between the source, the lithography scanner, through which the EUV light is focussed by the collector mirror.

The spectra were measured from a view-port positioned 90° to the drive laser axis using a broadband transmission grating spectrometer [24, 35, 36]. The spectrometer was operated with a 50 μm-wide entrance slit and a near-normal-incidence 10 000 lines mm^{-1} grating resulting in an instrument resolution of 0.11 nm full-width-at-half-maximum at a wavelength of 13.5 nm [24]. The diffracted light was subsequently recorded by a back-illuminated charge coupled device (CCD) from Princeton Instruments (PIXIS-XO: 2KB) with 2048 × 512 pixels. The camera was cooled to −17 °C to reduce the thermal noise. The spectrometer was aligned to observe the zero-order light close to the edge of the camera to

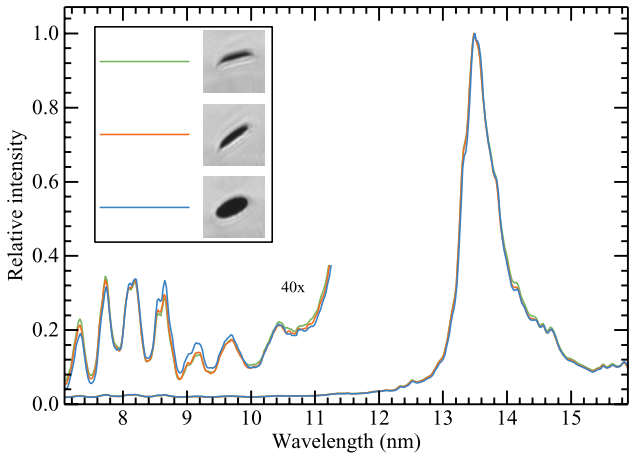

Figure 2. Three normalized spectra obtained under the same experimental conditions except for the target tilt. Shadowgraphic images of the pre-deformed target, obtained at 90° with respect to the main drive laser and show in the figure legend the different tilts just before the main pulse arrival. The short-wavelength emission features are magnified by a factor 40 to be visible on the same scale.

help with the wavelength calibration. The camera integration time was set to 12 ms, and therefore each spectrum is the result of averaging approximately 600 EUV shots. The average fluctuations of the overall amplitude of the spectra was found to be within ±3%. For each source setting, dark background frames were recorded by placing on the spectrometer line of sight a Si window of 2 mm thickness that absorbs light below 1.1 μm wavelength. These background frames were then subtracted from the recorded spectra to eliminate the dark counts and read-out noise. The resulting images were cropped and averaged over the non-dispersive axis to yield the raw spectra. The dispersive axis of the raw spectra was calibrated using the geometrical parameters of the spectrometer and applying the grating equation, obtaining a wavelength calibration uncertainty of 0.02 nm. The intensity axis of the spectra was corrected for the diffraction efficiency of the grating and quantum efficiency of the camera [37].

3. Results

Spectra obtained at different laser fluences are shown in figure 3. The dominant contribution to the spectrum is clearly the narrow emission feature centered around 13.5 nm wavelength. This emission feature is composed of thousands of atomic transitions in the ions Sn^{8+}–Sn^{14+} [12, 13, 15, 20, 24], which are clustered together in what are commonly known as unresolved transition arrays (UTAs) [38]. The lower charge states Sn^{8+}–Sn^{10+} mainly radiate photons with wavelengths longer than 13.5 nm [13, 20], whereas the ions Sn^{11+}–Sn^{14+} contribute to radiation in the 2% reflectivity bandwidth [15, 20].

Due to the changes in total emission intensity, relative changes between the spectra are better observed by normalizing each data set to its maximum value. In this representation, many interesting different aspects of the main emission feature become immediately apparent. Most laser fluences produce spectra with only very minor differences, with the exception of the lowest fluence in which the stronger contribution of lower charge states is observed in the long-wavelength tail of the emission. The features observed in this portion of the spectrum are well matched to strong transitions in Sn^{8+}–Sn^{10+} [13, 20].

The short-wavelength emission features between 7 and 11 nm, despite their much lower emission intensity, show much more drastic changes than the main feature at 13.5 nm. Moreover, the features observed in this region are charge state resolved even for the ions Sn^{11+}–Sn^{15+} [28], allowing for further information to be distilled. The spectrum produced by the lowest laser fluence is easily recognized by the stronger contribution from lower charge states Sn^{9+}–Sn^{11+} [28]. The strong presence of these charge states in both the main feature and the short wavelength region clearly indicates that the plasma temperature is too low for optimal source performance. Higher temperatures are necessary in order to increase the plasma average charge state and improve the source brightness at 13.5 nm.

Examination of the short-wavelength emission features also shows that, particularly when looking at emission from higher charge states, this spectral region is much more sensitive to laser fluence, and thus plasma temperature, changes. Therefore, the analysis of the features in the 7–11 nm range can be valuable to infer properties of the laser-produced plasma. This analysis is performed by employing the atomic data calculated in [28], where more detail on the atomic structure responsible for the emission features can be found. In short, these features stem from electric dipole transitions to the ground configurations of the ions Sn^{8+}–Sn^{15+}. The strongest transitions are in the form of $4p \rightarrow 5s$ and $4d \rightarrow 5p$. To perform the present analysis, the transition energies and probabilities from the calculations in [28] are employed.

In order to properly compare the atomic data with experimental spectra, some sort of scaling argument for the populations of excited states should be invoked. In [28], local thermodynamic equilibrium (LTE) was used as, in the case of higher-density, 1 μm-wavelength-driven LPP, the collision frequencies overcome spontaneous emission rates. Griem's criterion [39] states that, for the transitions here investigated, equilibrium should exist for electron densities above few times 10^{20} e^- cm^{-3}. In the present case, the strong reduction of the relevant plasma density due to the longer wavelength of the CO_2 drive-laser effectively breaks this assumption. In general, one would need a full collisional-radiative modelling approach, including the detailed atomic structure of all ions participating and all the relevant atomic plasma processes connecting said ions and their energy levels. This approach is extremely challenging and very computationally expensive, and lies beyond the scope of this work. For simplicity, the following approximations are used: first, using the non-equilibrium code FLYCHK [29], the average charge state as a function of electron temperature is calculated for a 10^{19} e^- cm^{-3} plasma; the level populations of each charge state are then weighted as if in LTE, applying the temperature found from FLYCHK. This approach may be expected to under- or overestimate the actual population of excited states but, when looking only at relative intensities and given that the individual spectra

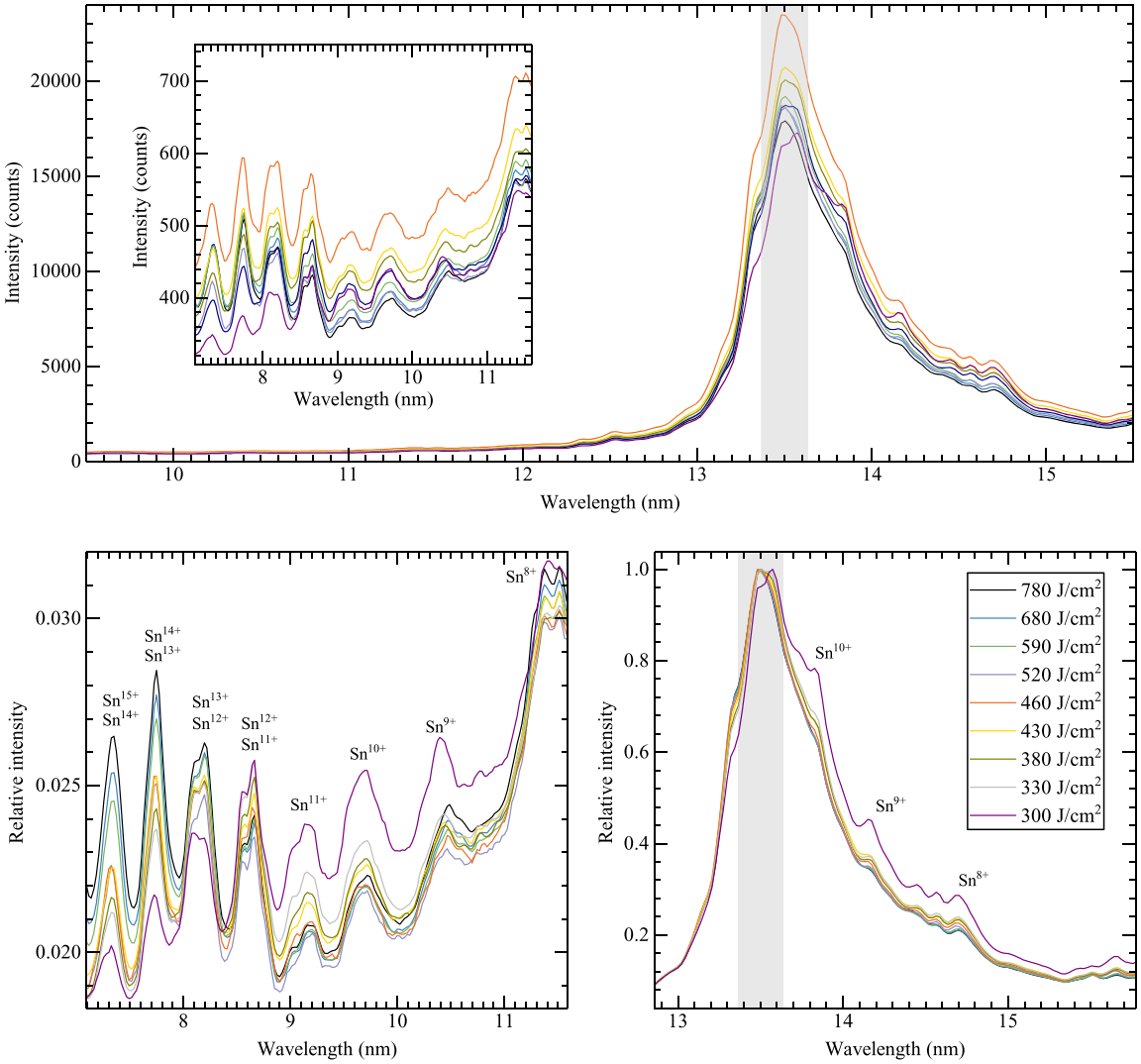

Figure 3. Top: absolute intensity spectra recorded for different laser fluences. Due to the large differences, the short wavelength emission features are presented in the appropriately scaled inset. Bottom: zoomed views for the short wavelength region and for the main emission feature, both normalized to the peak intensity at 13.5 nm. The gray shaded areas highlight the 2% band around 13.5 nm.

extends over a very limited wavelength range, the errors introduced should be tolerable. FLYCHK has been used in numerous experiment-calculation comparisons in recent years (see [29] and references therein). These comparisons show that FLYCHK provides meaningful estimates of ionization distributions.

The calculated spectra for the charge states Sn^{9+}–Sn^{15+} are shown in figure 4, already weighted using the appropriate Boltzmann factors (as determined from FLYCHK temperatures). Note that these calculated spectra have been manually shifted on average by 0.05 nm to match the experimentally observed features to ensure the convergence of the fitting procedure described in the following.

These spectra are subsequently used as input in a non-linear least-squares fitting routine which employs seven free-fit-parameters, one for each charge state. A linear combination of the calculated spectra is obtained which matches the experimental spectra. This procedure is quite robust, converging successfully for all spectra. An exemplary fitting result is shown in figure 4. The gray shaded area represent the continuum pedestal on which the atomic line emission rests. This continuum needs to be introduced as another fit-parameter to ensure the convergence of the fit. For the typical plasma densities and temperatures of a CO_2-produced-plasma, there is no clear physical reason for continuum radiation to exist as bound–bound transitions fully dominate emissivity. It is worth pointing out that the continuum levels almost perfectly correlate to the total amount of light recorded by the camera, which might then indicate the presence of stray light inside the spectrometer. Regardless of the underlying cause, the presence of the continuum pedestal does not affect the results of the analyses here presented.

From the fit parameters it is possible to extract the radiative contribution of each charge state to the short-wavelength range, see figure 5. These calculated contributions act as a simple proxy for the charge states populations in the LPP. The mean relative systematic deviation between model fit and experimental data, after removal of the continuum emission, is $\overline{|f(x)-y|/y} = 15.1\%$, i.e. 85% of the emission is well captured by our model. Some of the results show limitations of the method here employed. Firstly, the contributions from

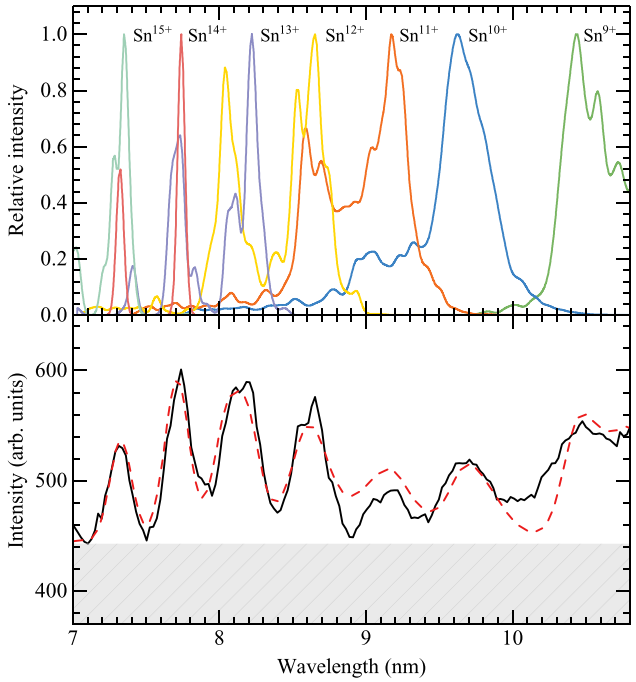

Figure 4. Top: individual charge state spectra calculated with the atomic data from [28] and weighted using Boltzmann statistics (see main text). Bottom: exemplary case, showing the result of fitting the short wavelength region to the spectrum obtained at 460 J cm^{-2}. Solid black line: experimental spectrum; dashed red line: fitted spectra; gray shaded area: fitted continuum level (see main text).

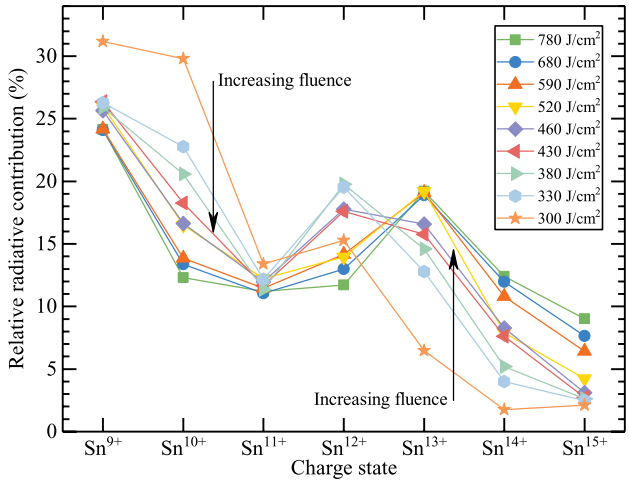

Figure 5. Relative radiative contribution of each charge state to the emission between 7 and 11 nm as determined from the fitting procedure for all laser fluence values.

lower charge states, in particular that from Sn^{9+}, seem to be overestimated. This could be due to the fact that these emission features are on top of the left-hand shoulder of the main emission feature centered at 13.5 nm. This extra contribution beneath would make them appear brighter. Secondly, the contribution from Sn^{11+} is fairly constant for all laser fluences, which could be an artifact from our fitting procedure. Moving towards the higher charge states, the contributions obtained however seem to be well-suited to qualitatively describe the change in charge state populations due to

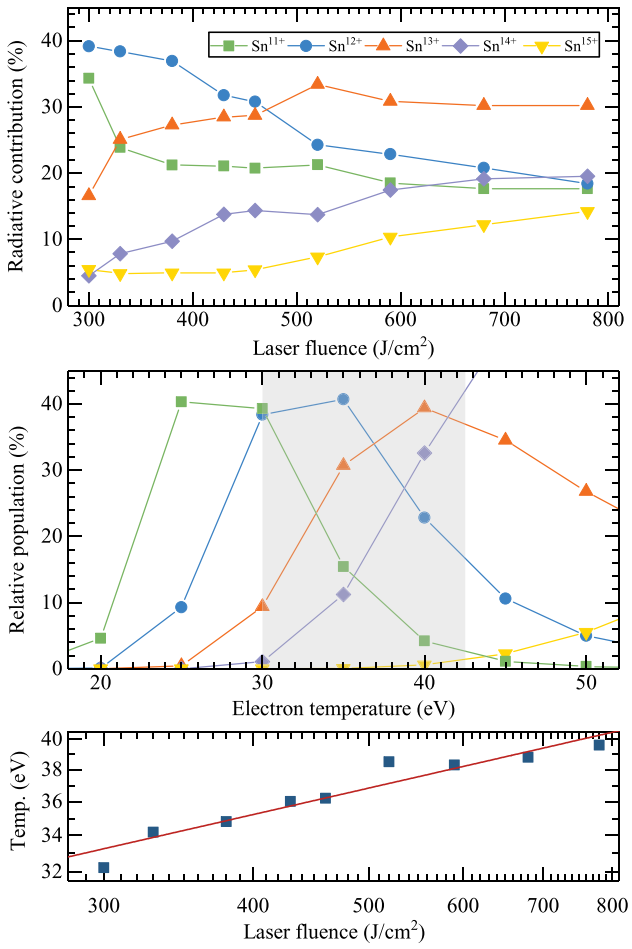

Figure 6. Qualitative comparison between the fitting procedure and FLYCHK calculations. Top: relative radiative contribution of the charge states Sn^{11+}–Sn^{15+}. Middle: relative charge state population from FLYCHK as function of electron temperature for a 10^{19} e$^-$ cm^{-3} density. The gray shaded area highlights the portion of the calculation that correlates to the range of experimental data shown in the upper panel. Bottom: scaling of electron temperature with laser fluence as deduced from the ratio of Sn^{13+} contribution to that of Sn^{12+} (see main text). The red solid line shows $T \propto F^{0.2}$.

changing laser fluence, and thus, changing plasma temperature. For this reason, we will now focus on these contributions and compare the corresponding fit results to the relative charge state populations as function of plasma temperature as obtained from FLYCHK calculations for a plasma with 10^{19} e$^-$ cm^{-3} electron density.

A comparison between the experimental data and the calculations is shown in figure 6, where the radiative contributions obtained from the fit results have been re-normalized for the charge states Sn^{11+}–Sn^{15+} such that their sum yields one for each experimental realization. When comparing these to the results from FLYCHK, it is seen that the general trends of the various charge states are well captured by the fitting procedure employed: Sn^{12+} contributions monotonically decrease from a 40% contribution value as laser fluence is increased; Sn^{13+} increases, then peaks at 520 J cm^{-2} before slowly falling again; Sn^{14+} and Sn^{15+} both monotonically increase over the measured range. Such behavior is observed also in

our calculations, indicating that a 30–42 eV temperature range was probed (shown as a shaded gray area in figure 6).

The dependence of the effective plasma electron temperature on the applied laser fluence can be deduced from these data, e.g. from the ratio between the contributions from Sn^{13+} and Sn^{12+}, by comparing our experimental results to FLYCHK calculations. We note that normalization factors and any associated systematic uncertainties identically drop out in this ratio. In the range observed, this leads to a monotonically increasing ratio Sn^{13+}/Sn^{12+} for both experimental data and results from calculations.

Through these calculations, each experimental point can be associated with a unique temperature value, and therefore a relationship between temperature and fluence is established as presented in the bottom panel of figure 6. A monotonic increase of temperature, in the range 30–40 eV, with laser fluence ranging 300–800 J cm^{-2} is observed. This suggests a surprisingly weak scaling $T \propto F^{0.2}$ of the effective plasma temperature T with fluence F. Recalling that in our framework fluence is a proxy for laser intensity (trivially, intensity $I \propto F$), this value can be compared to temperature-intensity relationships found in literature. The scaling found here is far weaker than the $T \propto F^{3/5}$ predicted by the collisional-radiative modelling approach [31] that is often cited in the literature. It is also lower than other approaches, such as the analytic results from Mora [40] resulting in a power of 4/9 or the 0.53 value found by Basko and coworkers [41]. Note that the aforementioned theory scaling powers do not include (changes in) radiative loss fraction [41, 42] which may lower the calculated value. On the other hand, the actual scaling may be expected to be weaker still as we use emission as a proxy of charge state balance, uncorrected for a hypothesized faster increase of the population of the more highly excited states with temperature. Such detailed calculations are however outside of the scope of the current work and are not expected to change our main conclusions. A partial explanation for the observed weak scaling may be found in the temporal shape of the laser pulse which first strongly peaks to decay over a longer, several-10 ns time scale. Thus, a wide range of instantaneous laser intensities is effectively probed in a single laser pulse and this may influence the effective, average, plasma temperature. A study of the possible influence from a spatial non-uniformity of the plasma would require full radiation-hydrodynamics modeling. Recent work by Schupp *et al* [43] however suggests that a single density and temperature approach is, in fact, apt. Care should be taken applying these results outside of the studied case as the scalings found are tied to the presented experimental conditions, namely the operational conditions of this EUV source.

4. Conclusions

The emission spectra in the 7–16 nm range from an industrial EUV light source are presented. The short-wavelength emission features in the 7–11 nm region are shown to strongly change with laser intensity and offer the possibility to individually diagnose several Sn charge states that strongly contribute to the main, unresolved emission feature at 13.5 nm wavelength relevant for nanolithography. Using the available atomic data for these emission features and the result of non-equilibrium plasma kinetics calculations with the code FLYCHK, synthetic spectra are generated for each charge state contributing in the 7–11 nm spectral region. The calculated spectra are then fitted to the experimental spectra, obtaining radiative contribution for each charge state. The changes of these contributions as function of the laser intensity are compared to the calculated charge state populations and their dependency on electron temperature. The data show that the effective plasma temperature is remarkably weakly dependent on laser intensity in the source here investigated.

Acknowledgments

The authors would like to thank ASML EUV System Power group and Proto-21 team for their support and thank Igor Fomenkov for in-depth technical discussions. The used transmission grating spectrometer has been developed in the Industrial Focus Group XUV Optics at University of Twente, and supported by the FOM Valorisation Prize 2011 awarded to F Bijkerk and NanoNextNL Valorization Grant awarded to M Bayraktar in 2015. Part of this work has been carried out at the Advanced Research Center for Nanolithography (ARCNL), a public-private partnership of the University of Amsterdam (UvA), the Vrije Universiteit Amsterdam (VU), the Netherlands Organisation for Scientific Research (NWO) and the semiconductor equipment manufacturer ASML. This project has received funding from European Research Council (ERC) Starting Grant No. 802648 and is part of the VIDI research programme with project number 15697, which is financed by NWO.

ORCID iDs

F Torretti https://orcid.org/0000-0001-8333-7618
J Scheers https://orcid.org/0000-0002-3627-8755
W Ubachs https://orcid.org/0000-0001-7840-3756
R Hoekstra https://orcid.org/0000-0001-8632-3334
O Versolato https://orcid.org/0000-0003-3852-5227

References

[1] Wagner C and Harned N 2010 *Nat. Photon.* **4** 24
[2] Waldrop M M 2016 *Nature* **530** 144
[3] Fomenkov I, Schafgans A and Brandt D 2019 *Synchrotron Radiat. News* **32** 3
[4] Banine V Y, Koshelev K N and Swinkels G H P M 2011 *J. Phys. D: Appl. Phys.* **44** 253001
[5] Benschop J, Banine V, Lok S and Loopstra E 2008 *J. Vac. Sci. Technol.* B **26** 2204
[6] Fomenkov I *et al* 2017 *Adv. Opt. Technol.* **6** 173
[7] Kawasuji Y *et al* 2017 *SPIE Advanced Lithography* vol 10143 (International Society for Optics and Photonics) p 101432G
[8] Vaschenko G *et al* 2006 *Opt. Lett.* **31** 1214
[9] Wachulak P, Torrisi A, Bartnik A, Fok T and Fiedorowicz H 2017 *Appl. Phys.* B **123** 25

[10] Bijkerk F, Bruineman C, de Bruijn R, van der Westen S A, Huiting R and Stuik R 2006 *EUV Sources for Lithography* ed V Bakshi (Bellingham, WA: SPIE) ch 27, pp 721–34 ISBN: 9780819496256
[11] Versolato O O 2019 *Plasma Sources Sci. Technol.* **28** 083001
[12] O'Sullivan G *et al* 2015 *J. Phys. B: At. Mol. Opt. Phys.* **48** 144025
[13] Churilov S S and Ryabtsev A N 2006 *Phys. Scr.* **73** 614
[14] Churilov S S and Ryabtsev A N 2006 *Opt. Spectrosc.* **100** 660
[15] Churilov S S and Ryabtsev A N 2006 *Opt. Spectrosc.* **101** 169
[16] Ryabtsev A N, Kononov É Y and Churilov S S 2008 *Opt. Spectrosc.* **105** 844
[17] Tolstikhina I Y, Churilov S S, Ryabtsev A N and Koshelev K N 2006 *EUV Sources for Lithography* ed V Bakshi (Bellingham, WA: SPIE Press) ch 4, pp 113–48
[18] Ohashi H, Suda S, Tanuma H, Fujioka S, Nishimura H, Sasaki A and Nishihara K 2010 *J. Phys. B: At. Mol. Opt. Phys.* **43** 065204
[19] Colgan J, Kilcrease D, Abdallah J, Sherrill M, Fontes C, Hakel P and Armstrong G 2017 *High Energy Density Phys.* **23** 133
[20] Torretti F *et al* 2017 *Phys. Rev.* A **95** 042503
[21] Bajt S, Alameda J B, Barbee T W Jr, Clift W M, Folta J A, Kaufmann B and Spiller E A 2002 *Opt. Eng.* **41** 1797
[22] Huang Q, Medvedev V, van de Kruijs R, Yakshin A, Louis E and Bijkerk F 2017 *Appl. Phys. Rev.* **4** 011104
[23] Purvis M *et al* 2018 *Extreme Ultraviolet (EUV) Lithography IX* vol 10583 (International Society for Optics and Photonics) p 1058327
[24] Schupp R *et al* 2019 *Phys. Rev. Appl.* **12** 014010
[25] van Zwol P *et al* 2017 *Photomask Technology* vol 10451 (International Society for Optics and Photonics) p 104510O
[26] Liu K, Li Y, Zhang F and Fan M 2007 *Japan. J. Appl. Phys.* **46** 6568
[27] Yang G and Li Y 2012 *Extreme Ultraviolet (EUV) Lithography III* vol 8322 (International Society for Optics and Photonics) p 83222V
[28] Torretti F, Schupp R, Kurilovich D, Bayerle A, Scheers J, Ubachs W, Hoekstra R and Versolato O O 2018 *J. Phys. B: At. Mol. Opt. Phys.* **51** 045005
[29] Chung H K, Chen M, Morgan W, Ralchenko Y and Lee R 2005 *High Energy Density Phys.* **1** 3
[30] Fomenkov I 2016 *EUVL Workshop* ed V Bakshi
[31] Colombant D and Tonon G 1973 *J. Appl. Phys.* **44** 3524
[32] Reijers S A, Kurilovich D, Torretti F, Gelderblom H and Versolato O O 2018 *J. Appl. Phys.* **124** 013102
[33] Chen H, Wang X, Duan L, Lan H, Chen Z, Zuo D and Lu P 2015 *J. Appl. Phys.* **117** 193302
[34] Kurilovich D, Klein A L, Torretti F, Lassise A, Hoekstra R, Ubachs W, Gelderblom H and Versolato O O 2016 *Phys. Rev. Appl.* **6** 014018
[35] Goh S, Bastiaens H, Vratzov B, Huang Q, Bijkerk F and Boller K 2015 *Opt. Express* **23** 4421
[36] Bayraktar M, Bastiaens H M, Bruineman C, Vratzov B and Bijkerk F 2016 *NEVAC Blad* **54** 14
[37] Poletto L, Boscolo A and Tondello G 1999 *Appl. Opt.* **38** 29
[38] Bauche J, Bauche-Arnoult C and Klapisch M 1988 *Adv. At. Mol. Phys.* **23** 131
[39] Griem H R 1963 *Phys. Rev.* **131** 1170
[40] Mora P 1982 *Phys. Fluids* **25** 1051
[41] Basko M M, Novikov V G and Grushin A S 2015 *Phys. Plasmas* **22** 053111
[42] Kurilovich D, Basko M M, Kim D A, Torretti F, Schupp R, Visschers J C, Scheers J, Hoekstra R, Ubachs W and Versolato O O 2018 *Phys. Plasmas* **25** 012709
[43] Schupp R *et al* 2019 *Appl. Phys. Lett.* **115** 124101